2024,9(4s)

e-ISSN: 2468-4376

https://www.jisem-journal.com/

**Research Article** 

# Power Quality Improvement using Optimal Shunt Active Power Filter with Novel Tilt Derivative and Tilt Integral Controller

### A Surya Prakasa Rao1\*, K Padma2

- <sup>1\*</sup>Department of Electrical and Electronics Engineering, Sir C R Reddy College of Engineering, Eluru, Andhra pradesh, India, aspeee@sircrrengg.ac.in
- $^2$ Department of Electrical Engineering, Andhra University College of Engineering, Visakhapatnam, Andhra pradesh India.  $^*$ Corresponding Author: A Surya PrakasaRao
- \*Department of Electrical and Electronics Engineering, Sir C R Reddy College of Engineering, Eluru, Andhrapredesh, India, aspeee@sircrrengg.ac.in

#### **ARTICLE INFO**

#### **ABSTRACT**

Received: 10 Oct 2024 Revised: 24 Nov 2024

Accepted: 20 Dec 2024

any power topologies, such as microgrids (MG) or distributed generation (DG), mix many energy sources with different demand patterns and energy conversion techniques in the Smart Grid(SG).SGs employ power electronic devices, which cause load-side harmonics. These devices interrupt the supply current, deviating it from the fundamental signal. Adding renewable energy sources to the electrical grid and using grid-connected power electronics interfaces have also challenged power quality. Harmonic disturbance reduction and power quality enhancement are important in contemporary power systems. A Shunt Active Power Filter (SAPF) is recommended to regulate voltage and reduce harmonics by managing reactive power, and it also boosts the power factor. This research aims to evaluate harmonic disturbances in the SG and suggest a technique to reduce harmonic distortions and achieve a harmonic distortion level below 5% of the total harmonic distortion (THD). The fundamental contribution of this study is the creation of a complicated control strategy, the Tilt-Derivative (TD) and Tilt-Integral (TI) controller, which effectively regulates and produces switching pulses for the SAPF's Voltage Source Inverter (VSI). A unique metaheuristic algorithm called Dynamic Opposite Learning-based Enhanced Mountain Gazelle Optimisation optimises the controller settings with MATLAB/Simulink.

Keywords: TD&TI, THD, PCC, PI, SG

### 1. INTRODUCTION:

Power quality problems have become more important as demand changes over time and more renewable energy sources are added to modern grid-connected systems [1][2][3]. Shunt active power filters (SAPFs) have demonstrated potential in addressing power quality issues such as harmonic distortion [4], reactive power, and unbalanced loads [5]. Researchers have proposed specific control systems for SAPFs. These include the instantaneous reactive power theory [6], the synchronous reference frame theory [7], and the model predictive control [8]. These strategies, however, usually demand complex computations and might not yield the greatest outcomes in dynamic working contexts. Use of optimisation techniques has improved SAPF performance. For instance, particle swarm optimisation (PSO) [9] has optimised SAPF control gains, and genetic algorithms (GA) [10] have optimised SAPF parameters. Nonetheless, especially under nonlinear operating situations, these optimisation techniques may not always guarantee optimal performance. Recent studies have focused on the creation of hybrid optimisation techniques meant to enhance SAPF performance. For instance, researchers have devised a hybrid GA-PSO optimisation method to maximise SAPF's control gains and parameters [11]. Researchers also employ PSO and a hybrid artificial bee colony (ABC) algorithm to enhance SAPF performance [12][13]. This work proposes an ideal design and control plan for SAPFs that enhances power quality in grid-connected systems.

2024,9(4s)

e-ISSN: 2468-4376

https://www.jisem-journal.com/ Research Article

A hybrid optimization method is used to make the suggested method work best in all kinds of running conditions. This is done by optimizing the SAPF's parameters and control gains.

### 2. THEORETICAL BASIS:

Comprising a shunt active power filter, the power circuit and control circuit provide compensating current. Maintaining DC voltage and energy storage, the power circuit combines a DC-link capacitor and a PWM-based inverter. The control circuit controls the power circuit and keeps careful checks on changes in the harmonic current so producing the required current. The shunt active power filter's design is really simple. Before the filter is attached at the point of common coupling (PCC), the power system's current flow is outlined as follows

$$is = i_1 = i_1 + i_h \tag{1}$$

where is stands for the source current,  $i_l$  for the load current,  $i_{ll}$  for the load current's fundamental component, and  $i_h$  for the load current's harmonic component. The SAPF generates 180° phase shift harmonic compensation current and DC-link current (idc) to preserve DC-link voltage (Vdc) at the PCC. Figure 1[14] demonstrates how the power system's current flows with SAPF.

$$i_s = i_l = [i_{1l} + i_h] - i_c + i_{dc}$$
 (2)

DC-link currents are designated by  $i_{\rm dc}$  and injected compensation current by  $i_{\rm c}$ . The voltage across the DC-link capacitor regulates harmonic compensation current. Figure 1 depicts the sinusoidal current with fundamental frequency arising from the harmonic counterproductive current cancelling out with the nonlinear load when kept at the appropriate level

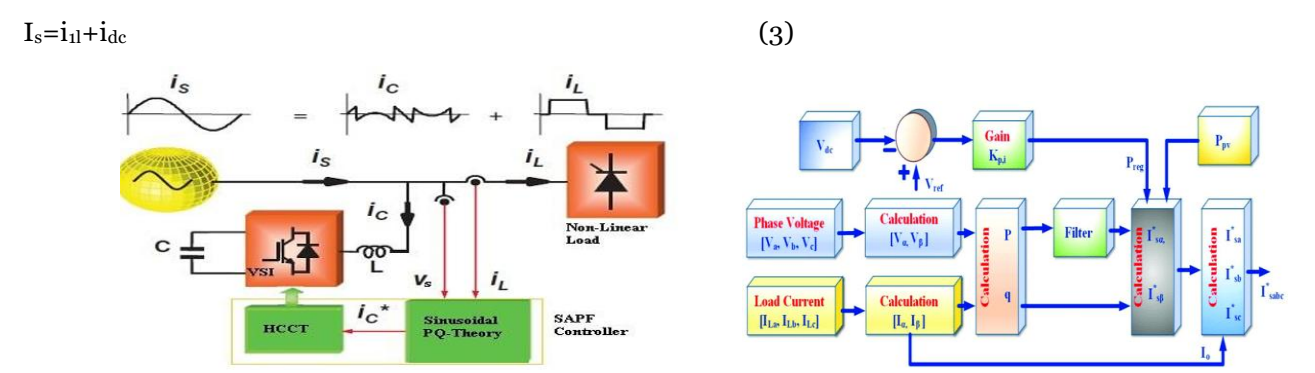


Figure 1. Fundamental Diagram of the SAPF Figure 2. Block diagram of the P&Q Power Theory

Harmonic extraction estimation significantly impacts shunt active power filter accuracy and efficiency. Either frequency domain analysis or time domain analysis can be used to find reference current; time domain analysis minimises control while frequency domain analysis utilises more memory. The work models simulations using MATLAB/Simulink to provide instantaneous reactive power theory (P-Q theory) in the time domain, as shown in Figure 2[15] With o-ALPH-components made from source voltages and currents, the Clarke transformation transforms stationary reference coordinates into rotating coordinates.

Where  $v_a$ ,  $v_b$ , and  $v_c$  refer to the three-phase voltages at the a-b-c coordinate,

 $i_a i_b$  and  $i_c$  represent the three-phase currents at the a-b-c coordinate,

 $v_0 v_\alpha$  and  $v_\beta$  are the three-phase voltages at the o- $\alpha$ - $\beta$  coordinate,

 $i_0$   $i_0$  and  $i_0$  refer to the three-phase currents at the o- $\alpha$ - $\beta$  coordinate.

The system considered in this paper is a three-phase three-wire system; therefore, a zero-sequence component is absent. In the  $\alpha$ - $\beta$  coordinate, the complex sum of the active and reactive powers (P and Q) can be represented by

$$S=P+jQ=v_{\alpha\beta}i_{\alpha\beta}^{*}=v_{\alpha}-jv_{\beta}i_{\alpha}+ji_{\beta}=v_{\alpha}i_{\alpha}+v_{\beta}i_{\beta}+jv_{\alpha}i_{\beta}-v_{\beta}i \tag{4}$$

2024,9(4s)

e-ISSN: 2468-4376

https://www.jisem-journal.com/ Research Article

S indicates the complex power; P means the active power; Q denotes the reactive power; \* denotes the complex conjugate. Consequently, one may characterise the components of instantaneous active and reactive power as P and Q respectively. For nonlinear loads, the components of instantaneous active and reactive power have been split into AC and DC forms. Whereas the AC component shows the energy transferred between the source and the load, the DC component shows the power delivered from the source to the load. The three-phase AC source supplies just the average DC component, which has been eliminated with a high-order low-pass filter.

$$P = p + p; Q = q + q (5,6)$$

Figure 3[16] shows the P-Q theory's power components. Using components of AC (p) and total reactive power (Q), the shunt active power filter generates harmonic reference currents.

It uses actual power from a three-phase AC source or external power supply to maintain DC-link voltage. The p-q Theory provides an efficient approach for harmonic extraction in SAPFs by calculating and separating instantaneous real and reactive powers. It allows for real-time compensation of harmonic currents, ensuring improved power quality and system stability. This work generates switching pulses for the voltage source inverter by use of hysteresis band current control. This technique is popular due to its straight forward topology, quick response, precision, and unconditioned stability. It uses a comparing the reference current to the actual current and switching the VSI on and off based on the mistake to preserve the actual current within the hysteresis band. Error is greater than the hysteresis band's upper limit. As shown in figure 4[17], the DC voltage usually rises to its highest value and falls to its minimum value when the output current must rise or fall.

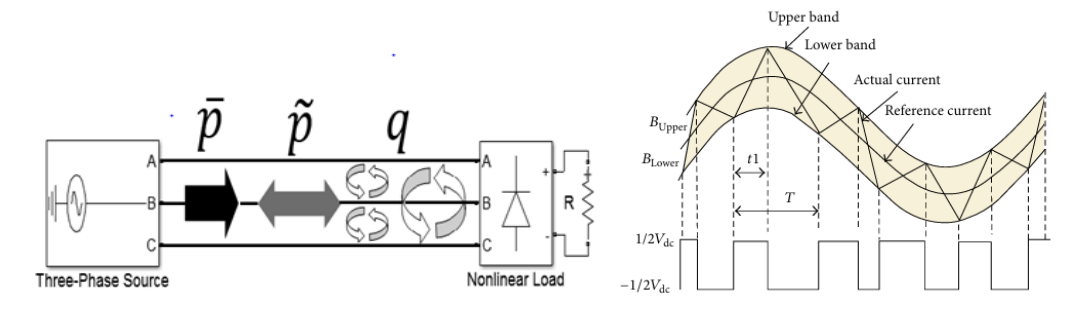


Figure 3. PQ diagram

Figure 4. Hysteresis Current Control Technique

# 3.0 METHODOLOGY:

Proposed TD&TI controller: Using DC-link voltage management, the shunt active power filter maintains a constant DC voltage on the DC side of the voltage source inverter. By means of voltage source inverters, DC-link capacitors build energy in power filters generating harmonic reference currents. The capacitor voltage has to be constant without power flow between the AC grid and the filter. As indicated, the voltage source inverter uses little actual power for switching. This work suggests an improved modified structure of the TID controller together with an efficient combination TD-TI controller. The TID controller is a fractional order controller (FOC) derived from the fractional-order calculus. Except the proportional parameter is slanted with a (1/s1/n), TID controller design is exactly PID controller construction. Due to the TID controller's ease of tuning, higher fluctuations rejection, and better sensitivity to system parametric alterations, this research proposed a TD-TI controller. The suggested TD-TI controller parameters are optimized using DOLMGO to improve power quality at PCC. As such, a TD-TI controller inside the DC-link voltage control loop guarantees a constant voltage and reduces harmonic current. Comparing DC-link capacitor voltage (vdc) to a reference DC voltage (vdc ref) and entering the error into the TD&TI controller helps to reduce the steady-state inaccuracy in reference signal tracking. The DC voltage TD&TI controller's internal current and outside voltage loops are shown below. Denoted as GPI(s) for the TD&TI controller and GVSI correspondingly are the transfer functions for each. When the VSI switches are operated at high frequency, (isa, isb,  $i_{sc}$ ) are approximately identical to  $(i_a, i_b, i_c)$ . Thus, the closed-loop current controller transfer function is unity.

2024,9(4s)

e-ISSN: 2468-4376

https://www.jisem-journal.com/ Research Article

In situations with considerable time delays or phase lags, Tilt Derivative and Tilt Integral [18] [19][20][21]Controllers increase system stability and performance. The Tilt Derivative controller uses a crossover frequency phase lead to reduce phase lag and stabilize the system. The Tilt Integral controller counter balances the phase lead with a crossover frequency phase lag, improving system stability and transient responsiveness. These controllers are employed for complicated systems with significant time delays, non-minimum phase behavior, or non-linearity when PID control is inadequate. Control theory, system dynamics, and the managed system's properties must be understood to develop and implement these controllers. Before real-world implementation, modeling, and testing assure system stability and effectiveness. Usually, the combined TD-TI controller's transfer function is written as follows.

$$G_{i1}, TD(S) = \frac{Kt_i}{\frac{1}{N}} + Kd_i$$
 (7)

$$G_{i2}, TI(S) = \frac{Kt_i}{\frac{1}{c_n}} + \frac{Ki_i}{s}$$

$$\tag{8}$$

$$total(s) = G_{i1}, TD(S) + G_{i2}, TI(S)$$
(9)

$$U_i(S) = G_i, total(s) * ACE_i(s)$$
(10)

In order to achieve the most effective adjustment of controller settings via the use of evolutionary algorithms, it is necessary to employ a suitable objective function. The optimum values of parameters are derived by minimizing the objective function with a unique metaheuristic algorithm called Dynamic Opposite Learning based Enhanced Mountain Gazelle Optimization optimization algorithm. In this work, the objective function is defined as the integral of time multiplied by the absolute error (ITAE) of the deviation of voltage ( $\Delta V_{dc}$ ), as seen below.

$$J = ITAE = \int_0^{tsim} t. \left[\Delta V_{dc}\right] dt \tag{11}$$

Where t sim the simulation time,

The optimization problem can be formulated as the minimization of the objective function J, subject to the given set of constraints.

$$K_X^{min} \le K \le K_X^{max} \tag{12}$$

Where x can denote  $k_{Ti}, k_{Di}, k_{Ti}, k_{Ii}$  of the TD and TI gains respectively,  $K_X^{min}$  and  $K_X^{max}$  are the Minimum and Maximum values of the employed TD&TI controller gain.

### 3.1 Proposed dynamic-opposite enhanced Mountain Gazelle Optimizer (DOLMGA)

Opposition-based learning (OBL)[22][23] is a successful strategy for improving algorithm searching by computing the opposite solution simultaneously. It enhances candidate solutions by bringing them closer to the best solution. Opposite number: OBL is a learning strategy based on the opposite number Xo.We define X as a real number,  $X \in [a, b]$ . The opposite number Xo can be defined as (13), where a and b are the boundaries.

$$X^0 = a + b - X \tag{13}$$

Opposite point: When  $X=(X1,X2,\ldots,XD)$  is a point in a Dimensional space,  $Xj,\ldots,XD\in[$  aj, bj ]; aj and bj are the low and high boundaries of the current population respectively, both of which change along with the iteration. A multi-dimensions opposite point is defined as

$$Xoj = aj + bj - Xj, \quad j = 1 : D$$
 (14)

### 3.2 The mathematical model of DOL

The dynamic opposite learning (DOL)[24] strategy optimizes a dynamic-opposite point (X) in a D-dimensional space using the DOL-based MGO optimization algorithm (DOLMGO). It involves population initialization and generation jumping, preventing premature convergence in complex problems. DOLMGO is a variant of TLBO that combines DOL population initialization and generation jumping.

2024,9(4s)

e-ISSN: 2468-4376

https://www.jisem-journal.com/ Research Article

3.3 Mountain Gazelle Optimizer (MGO): Mountains Gazelle Optimiser (MGO[25] and other natural-inspired optimisation techniques shine in tackling difficult tasks. Though MGO shows good results in many tasks, its performance in high-dimensional problems might be improved for real-world situations with significant variables. Natural occurring on the Arabian Peninsula, mountain gazelles have a low population density and strong territorial behaviour. Young men, mothers, and young and single men make three groups: Male and female gazelles fight more fiercely; young males use their horns more regularly. With an average pace of 80 km/h, mountain gazelles cover than 120 km in more auest food. Modelling of MGO: The MGO optimisation algorithm is a mathematical model inspired by mountain gazelle social interactions and surroundings. Crucially important elements of the social dynamics of the gazelles are the behaviour of bachelor male herds (BMH), maternity herds (MH), territorial and solitary males (TSM), and their migration pattern in search of food (MSF). These components are theoretically expressed as follows. Equation (1) approximates the mechanism by which adult male gazelles defend their territory from attackers.

$$TSM = male_{gezelle} - \left| \left( ri_1 * BH - ri_2 * X(t) \right) * F \right| * Cof_r$$
 (15)

Where  $ri_1$  and  $ri_2$ : are random integers of either 1 or 2. malegazelle:is the position vector of the best male gazelle so far. The values of BH ,F, and Cofr are determined using equations (14), (15), and (16).

$$BH = X_{ra} * r_1 + M_{pr} * r_2 \tag{16}$$

The value of  $X_{ra}$  is a random solution in the range of ra and that  $M_{pr}$  is the average of search agents.

N is the number of gazelles, and  $r_1$  and  $r_2$  are chosen at random from a range between 0 and 1.

$$F = N_1(D) * exp\left(2 - Iter\left(\frac{2}{MaxIter}\right)\right)$$
 (17)

The size of the problem dimension is represented by N1, and it is decided by a standard distribution. The iteration count and the maximum iterations are represented, respectively, by the Iter and MaxIter.

$$Cof_{1} = \begin{cases} (a+1) + r_{3}, \\ a * N_{2}(D), \\ r_{4}(D), \\ N_{3}(D) * N_{4}(D)^{2} * cos((r_{4} * 2) * N_{3}(D)), \end{cases}$$
(18)

where  $r_3$  and  $r_4$  stand for random numbers between 0 and 1;  $N_2$ ,  $N_3$ , and  $N_4$  are a collection of variables that were created at random and correspond to the problem function's size. At each iteration, the value of a is calculated using equation below.

$$a = -1 + Iter * \left(\frac{-1}{MaxIter}\right) \tag{19}$$

Maternity Herd(MH): Equation (20) provides a mathematical representation of the reasoning that goes into a mother gazelle's decision to defend its young.

$$MH = (BH + Cof_{1,r}) + (ri_3 * male_{aazelle} - ri_4 * X_{rand}) * Cof_{1,r}$$
(20)

Where Xrand represents a vector position of a gazeller and only selected from the population. Integer's  $ri_3$  and  $ri_4$  are selected at random from (1,2).

**3.4.Bachelor Male Herds (BMH):** The young adult male gazelles establish their territories as part of their maturation phase and attempt to get female gazelles to join them. The behavior is modeled in the equation (21)

$$BMH = (X(t) - D) + (ri_5 * male_{qazelle} - ri_6 * BH) * Cof_r$$
(21)

Where X(t) is the gazelle's position vector for the current iteration. The numbers ri5, and ri6 are chosen at random from (1, 2); r6: is a value chosen at random from the range (0 1); Equation (22) is used to find the value of D.

$$D = (|X(t)| + |male_{aazelle}|) * (2 * r_6 - 1)$$
(22)

2024,9(4s)

e-ISSN: 2468-4376

https://www.jisem-journal.com/

**Research Article** 

**3.5.MSF) Migration in Search of Food**: Mountain gazelles use a roving foraging strategy to find their preferred green pasture. Equation (21) models this random movement).

$$MSF = (ub - lb) * r_7 + l \tag{23}$$

The lower search boundary and upper search boundary are denoted by lb and ub, respectively.  $r_7$ 's value is randomly selected between 0 and 1.

### 3.6. Proposed Algorithm & flow chart[27]

Proposed algorithm step wise

Inputs: iteration counter (Iter), maximum

Iteration (MaxIter), population size (N).

Output: gazelle's position, and its fitness value

Initialize dynamic opposite learning based

random gazelle populations, Xi(i=1, 2, ...N)

Evaluate the fitness values of the population.

While (Iter<MaxIter), do

For (every gazelle, Xi) do

Calculate TSM using equation (15)

Calculate MH using equation (20)

Calculate BMH using equation (21)

Calculate MFS equation (23)

Evaluate the fitness values of TSM, MH, BMH and MSF

End for

Output best gazelle, Xbest, and its fitness values

End while

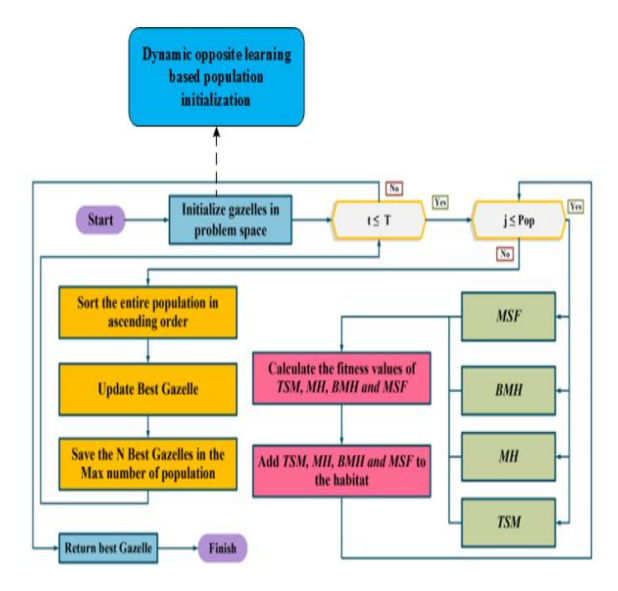


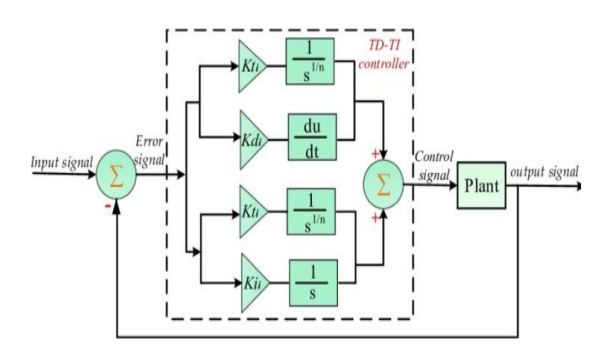
Figure 5. Proposed Algorithm flow Chart

2024,9(4s)

e-ISSN: 2468-4376

https://www.jisem-journal.com/

### **Research Article**



Figurem 6. TD &TI controller block diagram

**Table 1. Simulation Parameters** 

Utility Frequency	50 Hz
RMS utility voltages	100 V
$L_s$ – Grid side	0.15 mH
$R_s$ – Grid side	$0.1\Omega$
PV maximum Power $P_m$	305.226 W
$V_{oc}$	64.2V
$I_{sc}$	5.96A
Battery Nominal Voltage	1.2V
Rated Capacity	6.5 Ah
Fuel cell	65
- Number of cells	
Nominal stak efficiency	55%
Operating Temperature	65 Celsius
PV maximum Power $P_m$	305.226 W

# 4. SIMULATION RESULTS AND DISCUSSION

**4.1. Case-1.SAPF with PI controller:** The main block diagram of the test system is shown in Figure 7. Figure 8 provides the simulation diagram of the active power filter subsystem. From 0 seconds to 0.2 seconds, a balanced 3-phase system with a nonlinear load connects with a PI-controlled shunt active power filter. The trigger for the filter occurs at 0.04 seconds. Figure 9 illustrates the source voltage and the source current. Load nonlinearity, without compensation, modifies the source current from 0 seconds to 0.04 seconds. Figure 9 displays the source voltage and source current waveforms before and after the shunt active power. The filter is connected at the point of common coupling, along with the nonlinear load in a smart grid. The simulation parameters of the test system are presented in Table 1 [24].

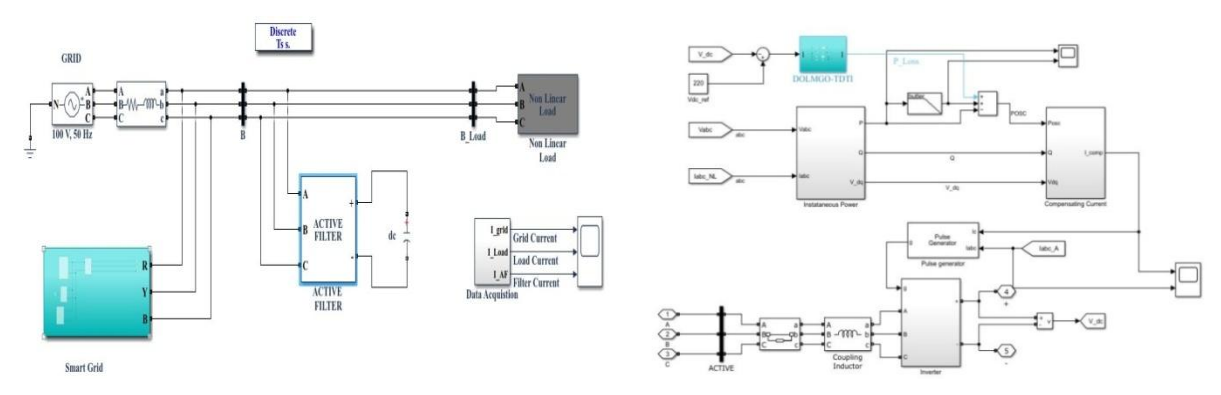


Figure 7.Simulation block diagram

Figure 8.Active Filter simaulation Subsystem

2024,9(4s)

e-ISSN: 2468-4376

https://www.jisem-journal.com/

**Research Article** 

Figure 10 shows load voltage and nonlinear load current (IL) waveforms. Figure 11 gives the variation in DC link capacitor voltage. The fast Fourier transform (FFT) analysis in Figure 12 shows that the source current has a total harmonic distortion (THD) of 26.72% without any compensation, which is higher than the IEEE harmonic standard limit. Total Harmonic Distortion (THD) has gone down from 26.72% to 2.68%, as shown by the FFT analysis in Figure 13. This is in line with the 5% IEEE standard with a PI-controlled shunt active power filter.

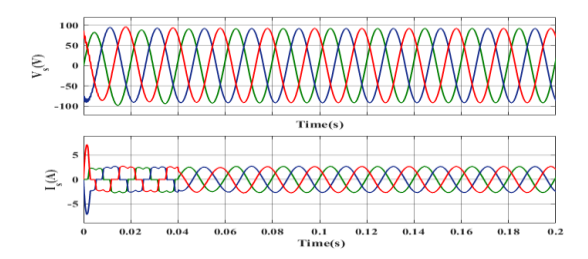


Figure 9.Source voltage &current variation

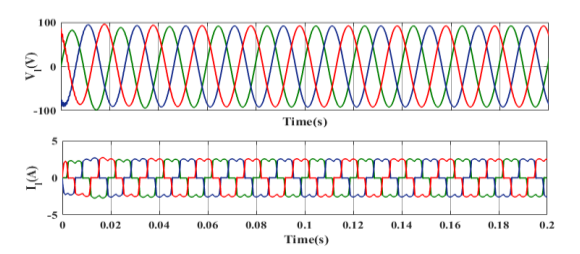


Figure 10.Load voltage &load current variation

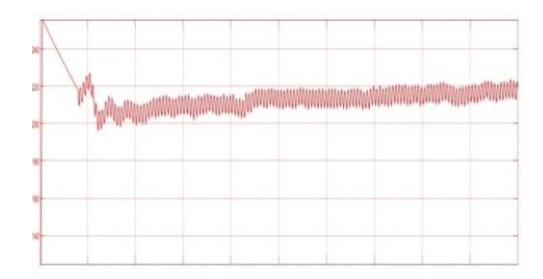


Figure 11.DC link capacitor voltage variation

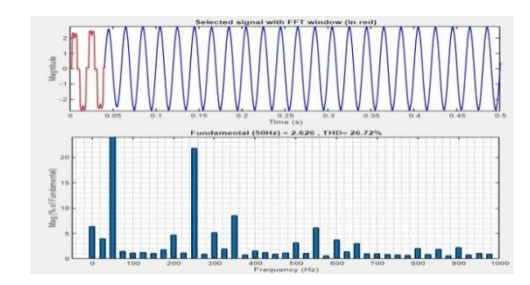


Figure 12.THD-FFT analysis without any compensation

Table 2. Proposed algorithm parameters.

Algorithm parameters	Maximum no of Iteration	Search Agent (N)		LB	UB
Value	50	3	4	0	1

**4.2. Case-2. SAPF With TD&TI Controller:** This section tests the TD&TI controller-based shunt active filter under balanced nonlinear load conditions. Source voltage and source current, load voltage, and load current waveforms are similar to case 1. The phase source current, load current, and filter current variation are given in Figure 14. Figure 15 shows the variation in the DC link capacitor voltage. Figure 16 shows the harmonic spectrum analysis for the system after compensation between 0.04 sec and 0.2 sec. The system has 1.06% total harmonic distortion, which is within the 5% IEEE standard.

**4.3.** Case 3: SAPF with optimal TD&TI controller: The controller's optimal TD&TI under consideration is The Matlab/Simulink environment effectively simulated the integration of renewable energy sources (PCC) through the utilisation of a three-phase boost converter. Table 1 gives the simulation parameters. Table 2 gives the algorithm parameters of the proposed Dynamic Opposite Learning-Based Enhanced Mountain Gazelle algorithm. Table 4.The table includes details about the diode bridge, details about the RL load, and optimal gains for the TD & TI controllers. The obtained results encompass various sources, including source current, load voltage, load current, and filter current, as well as FFT analysis for a three-phase power supply system. It is also clear that a

2024,9(4s)

e-ISSN: 2468-4376

https://www.jisem-journal.com/

#### **Research Article**

shunt active power filter is linked in parallel to both the power source and the load, which means that the load is nonlinear. The activation of the SAPF breaker occurs at a time interval of 0.04 seconds. The results show that all three scenarios-PI, TD&TI, and optimal TD&TI controllers based on SAPF-are the best at lowering harmonics in the current, raising reactive power, and making the power factor better. The system has 26.72% THD without a controller. Figure 13 shows that with the PI controller system, there is a 2.68% THD with the FFT study. The TD&TI controller decreases the THD to 1.06%, as shown in Figure 16, while the optimal TD&TI controller has THD reduced to 0.29%, as shown in Figure 19. A look at Table 3 shows how THD and power factor change over time when there is no compensation, PI, TD&TI, and optimal TD&TI controllers are used. Table 4 provides the diode bridge and RL load details. The best TD&TI controllers based on SAPF were able to reduce current harmonics, boost reactive power, and make the power factor better. Figure 17 represents the reactive power variation of the proposed method. Figure 18 shows the bar graph of THD with optimal TD & TI, TD & TI, PI, and without any controller. Figure 22 shows the convergence characteristics of the proposed system. The optimal TD&TI controller has THD reduced to 0.29%, as shown in Figure 19. Figure 20 displays the DC link voltage fluctuation with the optimal TD&TI controller. The DC link capacitor voltage changes more in the PI, TD, and TI controllers than in the best TD and TI controllers. Figure 21 gives the compensation current of the proposed method. Tables 3 and 5 show a full comparison of THD and power factor phase-wise, with and without compensation, PI, TD and TI controllers, and the best TD and TI controllers.

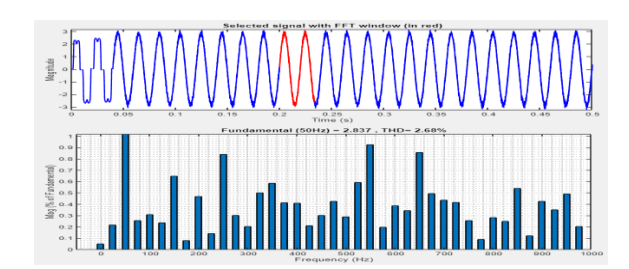


Figure 13.THD FFT analysis with PI controller

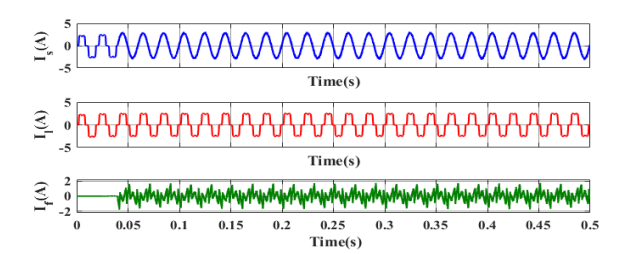


Figure 14. Source, load and filter currents per phase

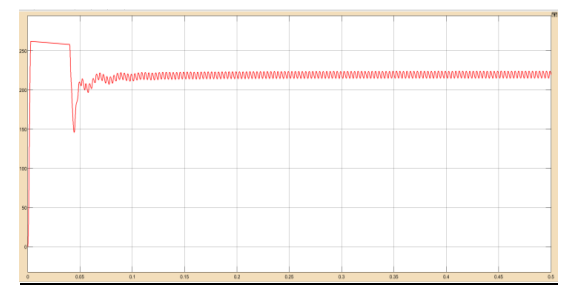


Figure 15.DC link capacitor voltage variation with TD&TI controller

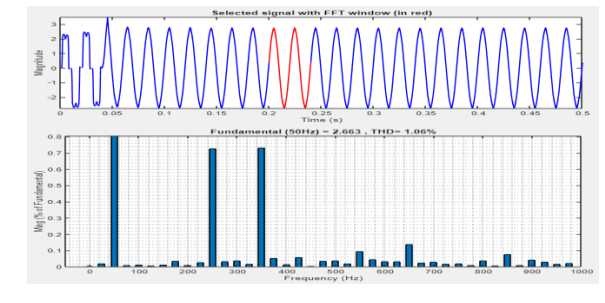


Figure 16.FFT analysis of THD after compensation with TD&TI controller

2024,9(4s)

e-ISSN: 2468-4376

https://www.jisem-journal.com/

### **Research Article**

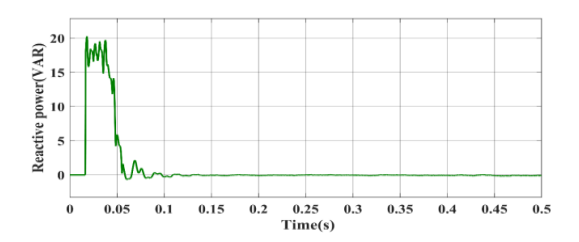


Figure 17.Reactive power variation of proposed method of the praposed method

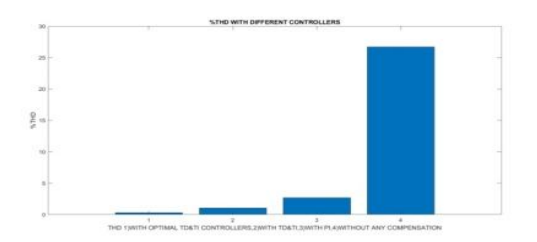


Figure 18.THD with optimal TD&TI,TD&TI ,PI and without any controller

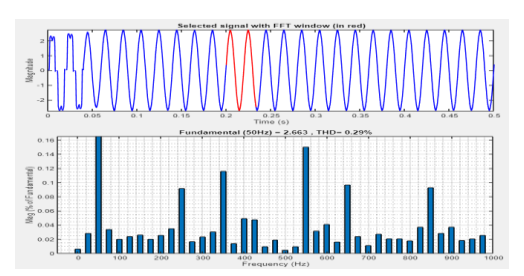


Figure 19. FFT with optimal TD&TI controller

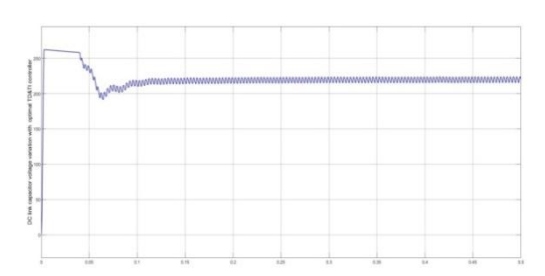


Figure 20.DC link capacitor voltage variation of the praposed method

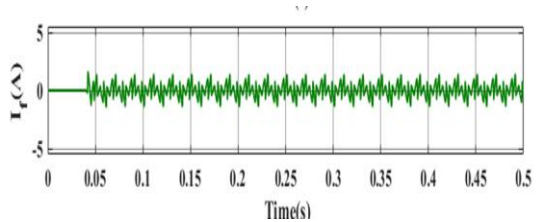


Figure 21 compensation current per phase

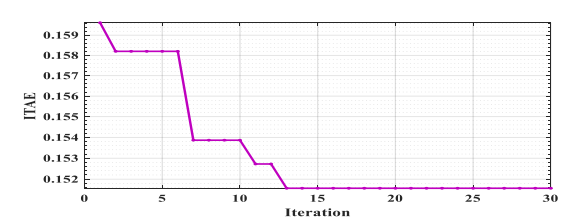


Figure 22. Convergence characteristicso of the proposed method

Table 3. Comparison of THD and power factor with phase wise, without compensation, with PI, with TD&TI, with optimal TD&TI controllers

THD Harmonic Order	Phases	$3^{th}$	$5^{th}$	$7^{th}$	$9^{th}$	$11^{th}$	13 <sup>th</sup>	15 <sup>th</sup>	17 <sup>th</sup>	19 <sup>th</sup>	THD%
w/o Compensation	A	1.04	21.82	8.52	0.94	6.08	3.03	0.72	1.88	1.05	26.72
	В	11.29	10.20	14.20	2.10	6.16	2.83	1.95	1.97	2.29	39.61
	C	12.82	19.54	14.50	2.35	6.06	1.97	2.54	1.21	1.92	47.79
PI	A	0.65	0.84	0.59	0.30	0.93	0.86	0.26	0.54	0.49	2.68
	В	0.32	0.64	0.57	0.40	0.58	0.49	0.27	0.51	0.84	2.25
	C	0.38	0.89	0.72	0.10	0.71	0.65	0.50	0.54	0.46	2.44
TDTI	A	0.01	0.73	0.73	0.00	0.09	0.14	0.02	0.08	0.02	1.06
	В	0.04	0.73	0.73	0.01	0.08	0.14	0.02	0.07	0.02	1.06
	C	0.02	0.71	0.74	0.01	0.07	0.15	0.00	0.08	0.03	1.05
With proposed	A	0.03	0.09	0.12	0.01	0.15	0.10	0.02	0.09	0.02	0.29
Controller(DOLMGO-	В	0.06	0.10	0.12	0.02	0.16	0.12	0.04	0.11	0.03	0.33
TDTI)	С	0.04	0.11	0.10	0.02	0.12	0.07	0.03	0.09	0.05	0.27

2024,9(4s)

e-ISSN: 2468-4376

https://www.jisem-journal.com/ Research Article

Table 4.Diode bridge, RL load details optimal TD&TI controller gains.

Nonlinear load	Three-phase diode bridge with RL load			
$R_L$	6οΩ			
$I_L$	20 mH			
$C_{dc}$	35μF			
Snubber resistance Rs	1e5 ohms			
Internal resistance	1e-3 ohms			
Ron				
Coupling Inductor- $L_c$	15mH			
	$K_t = 0.80295$			
Optimal-TDTI	$K_d = 0.015e-3$			
controller gains	$K_i$ = 0.4612			
	$K_n = 0.2971$			

Table 5. Power factor without compensation, with PI controller, with TD&TI controller, with optimal TD&TI controller

Techniques	Phases	Power factor		
	A	0.0373		
w/o Compensation	В	0.0252		
	C	0.0209		
	A	0.3495		
PI	В	0.4061		
	C	0.3792		
	A	0.6862		
TDTI	В	0.6862		
	C	0.6896		
With proposed	A	0.9604		
controller (DOLMGO-TDTI)	В	0.9496		
	С	0.9654		

### 5.0. CONCLUSION

The results obtained from conducting simulations on comparison case studies have provided validation that the proposed controller exhibits superior performance. We study a shunt active power filter with a optimal TD&TI controller to enhance power quality and assess system efficacy. Based on simulations, shunt active power filters get rid of harmonics and reactive current. This makes the source current sinusoidal and in phase with the source voltage. The total harmonic distortion (THD) of the optimal TD&TI controller-based shunt active power filter is less than 5%, which is in line with IEEE harmonic standards. It also has a shorter settling time. It also improves reactive power and power factor. We have finally concluded that optimal TD&TI controller-based shunt active filters have the capability to effectively mitigate harmonic currents, resulting in a notable decrease in total harmonic distortion (THD). In addition to reducing harmonics, it has to improve energy efficiency by adjusting for reactive power and keeping the system's power factor rather close to 1.

2024,9(4s)

e-ISSN: 2468-4376

https://www.jisem-journal.com/ Research Article

### **REFERENCES:**

- [1] S. K. Jain et al., "Power quality issues and their mitigation techniques," Journal of Electrical Systems, vol. 13, no. 2, pp. 147-164, 2017.
- [2] A review of active filters for power quality improvement. (1999, October 1). IEEE Journals & Magazine | IEEE Xplore. https://ieeexplore.ieee.org/document/793345
- [3] Popavath, L., & Kaliannan, P. (2018). Photovoltaic-STATCOM with Low Voltage Ride through Strategy and Power Quality Enhancement in a Grid Integrated Wind-PV System. Electronics, 7(4), 51. <a href="https://doi.org/10.3390/electronics7040051">https://doi.org/10.3390/electronics7040051</a>
- [4] Harmonics mitigation and power factor correction with a modern three-phase four-leg shunt active power filter. (2010, November 1). IEEE Conference Publication | IEEE Xplore. https://ieeexplore.ieee.org/document/5697574
- [5] Narasimhulu, V., Kumar, D. V. A., &Babu, C. S. (2019, May 7). Fuzzy Logic Control of SLMMC-Based SAPF Under Nonlinear Loads. International Journal of Fuzzy Systems; Springer Science+Business Media. <a href="https://doi.org/10.1007/s40815-019-00622-0">https://doi.org/10.1007/s40815-019-00622-0</a>
- [6] H. Akagi et al., "Instantaneous reactive power compensators comprising switching devices without energy storage components," IEEE Transactions on Industry Applications, vol. IA-20, no. 3, pp. 625-630, 1984.
- [7] A. Nabae et al., "A new scheme of compensation for reactive power and harmonics," IEEE Transactions on Industry Applications, vol. IA-22, no. 3, pp. 531-536, 1986.
- [8] J. Rodriguez et al., "Model predictive control of a shunt active power filter," IEEE Transactions on Industrial Electronics, vol. 55, no. 1, pp. 287-292, 2008.
- [9] A. K. Panda et al., "Particle swarm optimization-based shunt active power filter for power quality improvement," Journal of Electrical Systems, vol. 11, no. 2, pp. 141-152, 2015.
- [10] K. S. Suresh et al., "Genetic algorithm-based design of shunt active power filter," IET Power Electronics, vol. 7, no. 10, pp. 2511-2518, 2014.
- [11] S. K. Singh et al., "Hybrid genetic algorithm-particle swarm optimization for optimal design of shunt active power filters," IET Power Electronics, vol. 10, no. 11, pp. 1341-1350, 2017.
- [12] A. K. Panda et al., "Hybrid artificial bee colony algorithm-particle swarm optimization for optimal design of shunt active power filter," Journal of Electrical Systems, vol. 13, no. 2, pp. 165-176, 2017.
- [13] Reddy, C. R., Goud, B. S., Aymen, F., Rao, G. S., &Bortoni, E. C. (2021, September 14). Power Quality Improvement in HRES Grid Connected System with FOPID Based Atom Search Optimization Technique. Energies; Multidisciplinary Digital Publishing Institute. https://doi.org/10.3390/en14185812
- [14] Eid, A., Soliman, A., & Mehanna, M. (2023). DYNAMIC PERFORMANCE OPTIMIZATION OF SHUNT ACTIVE POWER FILTER TO ELIMINATE TOTAL HARMONIC DISTORTION. Journal of Al-Azhar University Engineering Sector, 18(66), 116–128. https://doi.org/10.21608/auej.2023.283033
- [15] Popavath, L., & Kaliannan, P. (2018). Photovoltaic-STATCOM with Low Voltage Ride through Strategy and Power Quality Enhancement in a Grid Integrated Wind-PV System. Electronics, 7(4), 51. https://doi.org/10.3390/electronics7040051
- [16] Imam, A. A., Kumar, R., & Al-Turki, Y. (2020, April 13). Modeling and Simulation of a PI Controlled Shunt Active Power Filter for Power Quality Enhancement Based on P-Q Theory. Electronics; Multidisciplinary Digital Publishing Institute. <a href="https://doi.org/10.3390/electronics9040637">https://doi.org/10.3390/electronics9040637</a>
- [17] Chelli, Z., Toufouti, R., Omeiri, A., & Saad, S. (2015). Hysteresis Control for Shunt Active Power Filter under Unbalanced Three-Phase Load Conditions. Journal of Electrical and Computer Engineering, 2015, 1–9. <a href="https://doi.org/10.1155/2015/391040">https://doi.org/10.1155/2015/391040</a>
- [18] Sahu, P. R., Simhadri, K., Mohanty, B., Hota, P. K., Abdelaziz, A. Y., Albalawi, F., Ghoneim, S. S. M., &Elsisi, M. (2023, January 12). Effective Load Frequency Control of Power System with Two-Degree Freedom Tilt-Integral-Derivative Based on Whale Optimization Algorithm. Sustainability; Multidisciplinary Digital Publishing Institute. https://doi.org/10.3390/su15021515
- [19] Sahu, R. K., Panda, S., Biswal, A., &Sekhar, G. T. C. (2016, March 1). Design and analysis of tilt integral derivative controller with filter for load frequency control of multi-area interconnected power systems. Isa Transactions; Elsevier BV. <a href="https://doi.org/10.1016/j.isatra.2015.12.001">https://doi.org/10.1016/j.isatra.2015.12.001</a>

2024,9(4s) e-ISSN: 2468-4376

https://www.jisem-journal.com/

**Research Article** 

- [20] Pahadasingh, S. (2022, April 12). Load Frequency Control of Multi Area System Incorporating Distributed Generation Resources Using Closed Loop Cascade of 3DOFPID-FPID-TID Controller. <a href="https://www.academia.edu/76280092/">www.academia.edu/76280092/</a> Load Frequency Control of Multi Area System Incorporating Distributed Generation Resources Using Closed Loop Cascade of 3DOFPID FPID TID Controller.
- [21] Elkasem, A. H. A., Khamies, M., Hassan, M. H., Agwa, A. M., &Kamel, S. (2022, April 13). Optimal Design of TD-TI Controller for LFC Considering Renewables Penetration by an Improved Chaos Game Optimizer. https://doi.org/10.3390/fractalfract6040220
- [22] Xu, Y., Yang, Z., Li, X., Kang, H., & Yang, X. (2019). Dynamic opposite learning enhanced teaching—learning-based optimization. Knowledge-Based Systems, 188, 104966. https://doi.org/10.1016/j.knosys.2019.104966
- [23] Xu, Y., Yang, Z., Liu, X., Kang, H., & Yang, X. (2020, January 1). Dynamic opposite learning enhanced teaching—learning-based optimization. Knowledge Based Systems; Elsevier BV. <a href="https://doi.org/10.1016/j.knosys.2019.104966">https://doi.org/10.1016/j.knosys.2019.104966</a>
- [24] A review of active filters for power quality improvement. (1999, October 1). IEEE Journals & Magazine | IEEE Xplore. https://ieeexplore.ieee.org/document/793345
- [25] Kumar, D. P. (2007). Investigations on shunt active power filter for power quality improvement. http://ethesis.nitrkl.ac.in/4306/

### **BIOGRAPHIES OF AUTHORS**



Sri A.surya prakasa rao received B.Tech degree in electrical and electronics engineering from Kakatiya University, Warangal ,Andhra Pradesh(AP) in 2001,M.Tech degree from JNTU-Kakinada-AP, in 2005.Presently he is pursuing P.hd at Andhra university, Visakhapatnam-AP, India .Currently he is working as a Sr.assistant professor ,in the department of in electrical and electronics engineering, Sir C R R College of engineering ,Eluru, AP, India .His research interests include Power quality improvement,FACTS, Power system optimization ,smart grids, renewable energy sources.

Email: aspeee@sircrrengg.ac.in

ORCID ID: 0000-0003-1201-9772

Researcher ID:LZI-0576-2025



Dr. Kottala Padma received B.Tech (2005) in Electrical and Electronics Engineering from Sri Venkateswara University, Tirupathi, M.E degree (2010), and Ph.D (2015) from Andhra University, Visakhapatnam, Andhra Pradesh. Her research interests are Soft Computing Techniques, IOT technologies, Renewable Energy Systems, Micro grids.

Email: padma315@gmail.com

ORCID ID: https://orcid.org/0000-0003-2425-9167

Researcher id: AAP-4851-2930

Google scholar id: ublc7qAAAAAJ

Scopus id: 57189232675